Journal of Applied Physics

Development of Fe-based amorphous alloy with high iron content for room-temperature magnetic refrigeration application

Cite as: J. Appl. Phys. **132**, 055103 (2022); https://doi.org/10.1063/5.0098662
Submitted: 11 May 2022 • Accepted: 09 July 2022 • Published Online: 02 August 2022

Mengqi Gao, Lei Xie, Qiang Li, et al.

Journal of Applied Physics ARTICLE scitation.org/journal/jap

Development of Fe-based amorphous alloy with high iron content for room-temperature magnetic refrigeration application

Cite as: J. Appl. Phys. **132**, 055103 (2022); doi: 10.1063/5.0098662
Submitted: 11 May 2022 · Accepted: 9 July 2022 ·
Published Online: 2 August 2022

Mengqi Gao,[1,2] Lei Xie,[1,2] Qiang Li,[1,2,a)] Juntao Huo,[3,b)] and Chuntao Chang[4,c)]

AFFILIATIONS

[1]Xinjiang Key Laboratory of Solid State Physics and Devices, Xinjiang University, Urumqi, Xinjiang 830046, China
[2]School of Physics Science and Technology, Xinjiang University, Urumqi, Xinjiang 830046, China
[3]CAS Key Laboratory of Magnetic Materials and Devices, Ningbo Institute of Materials Technology and Engineering, Chinese Academy of Sciences, Ningbo, Zhejiang 315201, China
[4]School of Mechanical Engineering, Dongguan University of Technology, Dongguan 523808, China

[a)]**Author to whom correspondence should be addressed:** qli@xju.edu.cn
[b)]**Electronic mail:** huojuntao@nimte.ac.cn
[c)]**Electronic mail:** changct@dgut.edu.cn

ABSTRACT

In this work, in order to develop new Fe-based amorphous alloys with room-temperature magnetocaloric effect and good magnetocaloric performance, high iron content Fe-based amorphous alloys were designed, and their Curie temperatures were adjusted to room temperature through the addition of Mo. As a result, a new $Fe_{83}Mo_6Si_1B_7P_2C_1$ amorphous alloy with room-temperature magnetocaloric effect was successfully prepared by melt-spinning technique, and it has the Curie temperature of 300 K, the maximum isothermal magnetic entropy change of 2.74 J kg^{-1} K^{-1} and the refrigerant capacity of 485.2 J kg^{-1} under an applied magnetic field of 5 T. Combining with the advantages of excellent magnetocaloric properties, negligible hysteresis loss, and low material cost, the present $Fe_{83}Mo_6Si_1B_7P_2C_1$ amorphous alloy should be a promising candidate as room-temperature magnetic refrigerants.

I. INTRODUCTION

The traditional gas compression refrigeration technology has the disadvantages of low efficiency, high energy consumption, and serious pollution and, therefore, new refrigeration technologies are long-anticipated. In 1917, Pierre Weiss and Auguste Piccard announced the discovery of magnetocaloric effect, a phenomenon in which the temperature of a ferromagnet or paramagnetic material varies with the magnetic field during an adiabatic process.[1] Until 1997, $Gd_5(Si_xGe_{1-x})_4$ alloy with giant magnetocaloric effect was discovered by Pecharsky and Gschneidner.[2] Since then, magnetic refrigeration technology based on MCE has attracted wide public attention as a new refrigeration technology with the advantages of environmental protection, high efficiency, and low noise.[3–5] Magnetic refrigeration materials based on first-order phase transition often exhibit giant magnetocaloric effect. Some of the more famous ones include $Gd_5Si_2Ge_2$,[6] $La(Fe,Si)_{13}$,[7] and Heusler alloys.[8] But the full width at half the maximum of magnetic entropy change is rather small and usually less than 20 K, which results in a low refrigeration capacity (RC).[9] Amorphous alloys as magnetic refrigeration materials are based on second-order magneto-structural phase transformation (SOMT), which has some advantages compared to first-order magneto-structural phase transition (FOMT) materials, such as small magnetic and thermal hysteresis, broad operating temperature range, and large RC.[10,11] In addition, some of them are very soft magnetic materials and their Curie temperature can be easily adjusted by changing the chemical composition or/and conducting appropriate heat treatment.[12] Due to the huge demand of commercial market, room-temperature magnetic refrigeration has great research significance. Amorphous alloys used for room-temperature magnetic refrigeration can be

divided into two classes of rare-earth-metal (RE) based and transition-metal (TM) based amorphous alloys. The RE-based amorphous alloys usually exhibit large magnetic entropy change (ΔS_M),[13] but expensive materials cost and poor corrosion resistance. The TM-based, mainly Fe-based, amorphous alloys exhibit good thermal conductivity, high corrosion resistance, excellent mechanical properties, and low material cost. These advantages make Fe-based amorphous alloys have a broad application prospect as room-temperature magnetic refrigeration materials. However, in order to depress the T_C of Fe-based amorphous alloys to near room temperature, some elements with antiferromagnetic coupling with Fe have to be added, which leads to the low ΔS_M and *RC*.[14] Therefore, it is of great significance to develop a new strategy for the development of Fe-based amorphous alloys with excellent room-temperature magnetocaloric properties.

It is generally recognized that the value of ΔS_M of an alloy is proportional to its saturation magnetization (M_s).[15,16] Since the ferromagnetism of Fe-based amorphous alloys is mainly provided by Fe atoms, Fe-based amorphous alloys with higher Fe content can be expected to have higher M_s and, thus, a larger ΔS_M. Additionally, previous studies[17–20] have found that the T_C of some Fe-based amorphous alloys decreases with an increase in Fe content when Fe content is larger than 80 at. %. Therefore, it is desirable to develop room-temperature magnetic refrigeration material with large ΔS_M based on Fe-based amorphous alloys with high Fe content.

To develop Fe-based amorphous alloys with a large ΔS_M for room-temperature magnetic refrigeration application, we focus on Fe-based amorphous alloys with high Fe content and adjust its T_C by adding Mo element in this work. Finally, a new $Fe_{83}Mo_6Si_1B_7P_2C_1$ amorphous alloy with high iron content and a T_C of 300 K was successfully prepared by melt-spinning technique, and its magnetocaloric properties were further investigated.

II. EXPERIMENT PROCEDURES

The mother alloy ingots of $Fe_{89-x}Mo_xSi_1B_7P_2C_1$ (x = 5, 6, 7 at. %) were prepared by arc-melting mixtures of pure Fe (99.99 wt. %), Mo (99.99 wt. %), Fe_3P (99.5 wt. %), Si (99.95 wt. %), B (99.5 wt. %), and graphite (99.9 wt. %) under an argon atmosphere. Then, the ribbon samples with a width of 1–2.5 mm and a thickness of 15–25 μm were prepared by single-roller melt-spinning at a wheel speed of 50 m/s under an Ar atmosphere.

The phase structure of the ribbon samples was determined by an x-ray diffractometer (XRD, Bruker D8 advance diffractometer) with Cu K_α radiation at room temperature. The hysteresis loop of the samples was measured by a vibrating sample magnetometer (VSM, Lakeshore 7404) with the maximum applied field of 800 kA/m at a temperature of 100 K. The temperature and field dependences of magnetization of the samples were measured using a superconducting quantum magnetometer (SQUID, MPMS XL-7). The curve of the isothermal magnetic entropy change vs temperature (ΔS_M–T curve) under different applied fields was obtained from isothermal magnetization curve at different temperatures using the Maxwell relation,[21] and the *RC* is defined as the product of the half-height width at the maximum ΔS_M of the material and the maximum ΔS_M.[15]

III. RESULT AND DISCUSSION

Figure 1 presents the XRD patterns and the DSC curves of as-spun $Fe_{89-x}Mo_xSi_1B_7P_2C_1$ (x = 5, 6, 7 at. %) ribbons. As shown in Fig. 1(a), the XRD patterns of all the samples show a very typical wide diffraction peak at 2θ = 45° and no sharp crystallization peaks, indicating a completely amorphous phase. The DSC curves show a clear glass transition temperature (T_g), followed by an extended supercooled liquid region and a multi-stage of crystallization

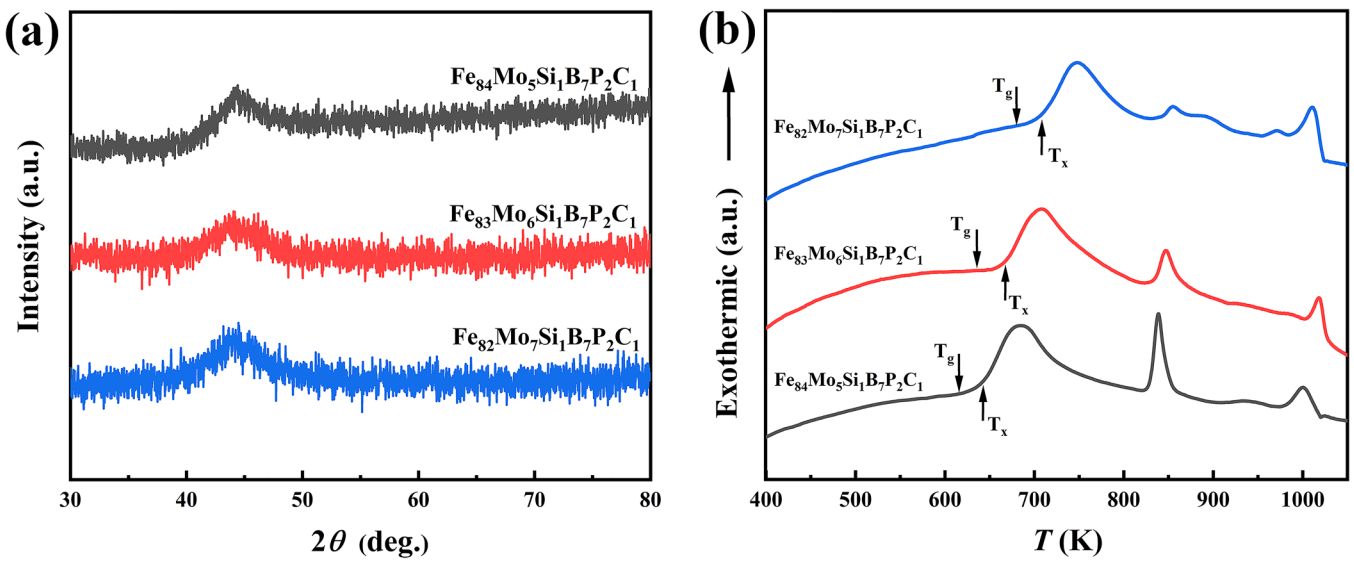

FIG. 1. The XRD pattern of $Fe_{89-x}Mo_xSi_1B_7P_2C_1$ (x = 5, 6, 7) amorphous alloy strip (a) and the DSC thermodynamic scanning curve at the heating rate of 0.33 K/s (b).

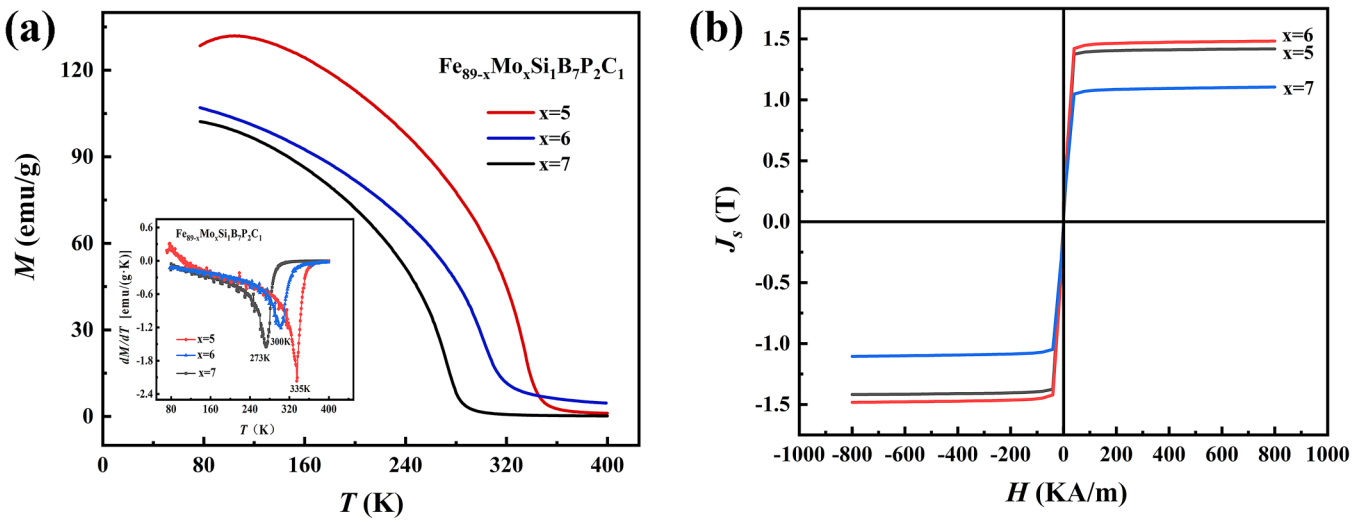

FIG. 2. M–T curves and corresponding d*M*/d*T*–*T* curves (inset) under an applied field of 0.02 T (a) and hysteresis loops at a temperature of 100 K (b) of the as-spun $Fe_{89-x}Mo_xSi_1B_7P_2C_1$ (x = 5, 6, 7 at. %) amorphous alloy ribbons.

process as the temperature increases, which further confirms the glassy nature of the samples.

Figure 2(a) shows the *M*–*T* curves and d*M*/d*T*–*T* curves (inset) under an applied magnetic field of 0.02 T for the as-spun $Fe_{89-x}Mo_xSi_1B_7P_2C_1$ (x = 5, 6, 7 at. %) amorphous ribbons. The T_C of the $Fe_{89-x}Mo_xSi_1B_7P_2C_1$ amorphous alloy can be determined from d*M*/d*T*-*T* curve to be 335, 300, and 273 K for x = 5, 6, and 7, respectively. It can see that the T_C of the present Fe-based amorphous alloys decreases with an increase in Mo content, which is due to the antiferromagnetic coupling between Mo and Fe atoms leading to the reduction in the exchange integral between magnetic atoms in the sample.[22] Figure 2(b) shows the hysteresis loop of the as-spun $Fe_{89-x}Mo_xSi_1B_7P_2C_1$ (x = 5, 6, 7 at. %) amorphous ribbons at a temperature of 100 K. It can be clearly found that the coercive force (H_c) of the three amorphous alloys is negligible, indicating a low hysteresis loss. It is notable

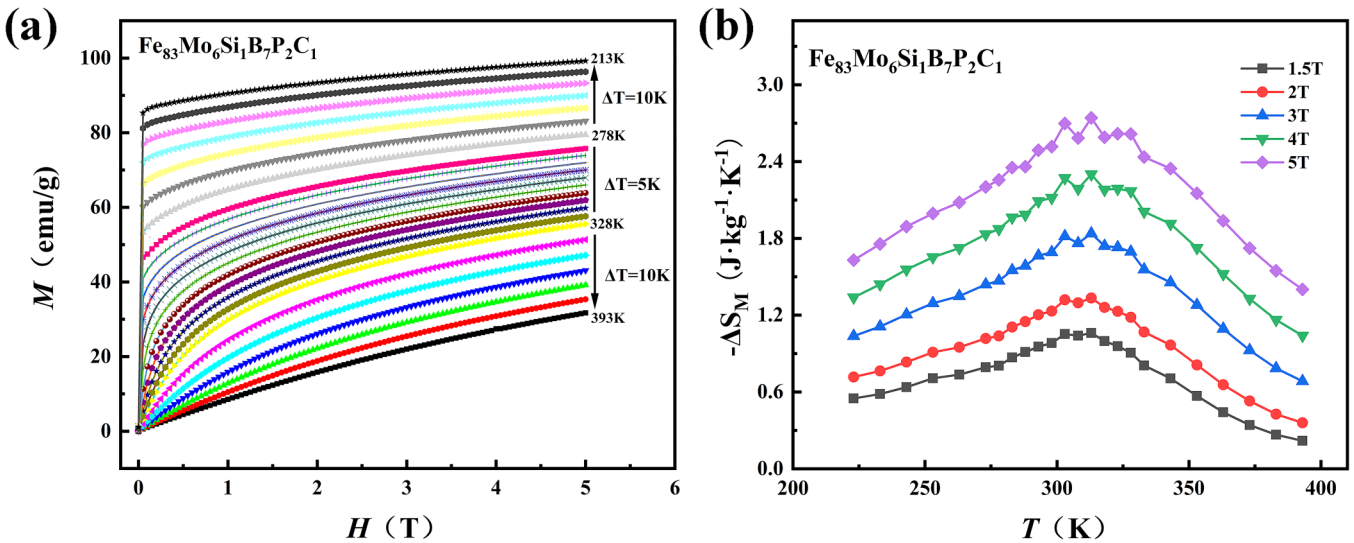

FIG. 3. Isothermal magnetization curve (a) in the temperature range of 213–393 K and the temperature dependence of magnetic entropy change (b) of the $Fe_{83}Mo_6Si_1B_7P_2C_1$ amorphous alloy ribbon.

TABLE I. Magnetocaloric properties of the present $Fe_{83}Mo_6Si_1B_7P_2C_1$ amorphous alloy and several reported Fe-based amorphous alloys with near room-temperature magnetocaloric effect.

			$\lvert\Delta S_M^{max}\rvert$ (J kg^{-1} K^{-1})		RC (J kg^{-1})		
Composition (at. %)	Material form	T_c (K)	1.5 T	5 T	1.5 T	5 T	Reference
$Fe_{83}Mo_6Si_1B_7P_2C_1$	Ribbon	300	1.06	2.74	138.2	485.2	This work
$Fe_{77}Ta_5B_{10}Zr_9Cu_1$	Ribbon	313	…	2.03	…	241.5	24
$Fe_{65}Mn_{15}P_{10}B_7C_3$	Ribbon	292	0.91	…	79.8	…	25
$Fe_{88}La_4Ce_3B_5$	Ribbon	303	1.54	3.93	201	715.3	26
$Fe_{86}Zr_{11}B_3$	Ribbon	300	0.77	…	77	…	27

that the $Fe_{83}Mo_6Si_1B_7P_2C_1$ amorphous alloy possesses the highest saturation magnetization (J_s) of 148 emu/g among the present Fe-based amorphous alloys. Due to the antiferromagnetic coupling between Mo and Fe atoms, it is understandable that the J_s of the alloy with x = 7 is less than that of the alloys with x = 5 and 6. However, it is anomalous that the J_s of the alloy with x = 6 is larger than that of the alloys with x = 5. It is known that the exchange integral between magnetic atoms strongly depends on their distance. It is known that the position of Fe on the Bethe–Slater curve lies on the left side of the maximum due to the small atomic diameter of Fe.[23] The atomic diameter of Mo (0.136 nm) is larger than that of Fe (0.124 nm), so the addition of Mo may increase the average atomic distance between Fe atoms in the present Fe-based amorphous alloys and thus leads to the enhancement of the exchange integral between Fe atoms, which may cancel out the effect of the antiferromagnetic coupling between Mo and Fe atoms and result in the slight increase in the J_s.

Because $Fe_{83}Mo_6Si_1B_7P_2C_1$ amorphous alloy has a T_C near room temperature and the largest J_s, its magnetocaloric properties are further investigated. Figure 3(a) shows M–H curves of the $Fe_{83}Mo_6Si_1B_7P_2C_1$ amorphous alloy measured under different applied fields from 0 to 5 T at different temperatures near its T_C (300 K), in which the test temperature span is 213–393 K, and the test temperature interval is 5 K near the T_c and 10 K away from the T_C.

The ΔS_M of the sample can be calculated from M–H curves using the Maxwell relation,[11,21]

$$\Delta S_M(T, H) = \int_0^{H_{max}} \left(\frac{\partial M}{\partial T}\right)_H dH, \quad (1)$$

where H_{max} is the maximum applied field. In order to facilitate numerical calculation, the following equation is commonly used to calculate the ΔS_M:

$$\Delta S_M(T_i, H) = \frac{\int_0^H M(T_i, H)dH - \int_0^H M(T_{i+1}, H)dH}{T_i - T_{i+1}}. \quad (2)$$

The temperature dependence of ΔS_M for the $Fe_{83}Mo_6Si_1B_7P_2C_1$ amorphous alloy can be obtained as shown in Fig. 3(b). Its maximum ΔS_M ($\lvert\Delta S_M^{max}\rvert$) and RC are determined and listed in Table I. The $\lvert\Delta S_M^{max}\rvert$ and RC of the $Fe_{83}Mo_6Si_1B_7P_2C_1$ amorphous alloy ribbon under the applied field of 1.5 and 5 T are 1.06 and 2.74 J kg^{-1} K^{-1}, and 138.2 and 485.2 J kg^{-1}, respectively. Meanwhile, the magnetocaloric properties of several reported amorphous alloys with near room-temperature magnetocaloric effect are also listed in Table I. It can be seen that, compared with those reported amorphous alloys, the $\lvert\Delta S_M^{max}\rvert$ and RC of the present $Fe_{83}Mo_6Si_1B_7P_2C_1$ amorphous alloy are greater than those of most Fe-based amorphous alloys with near room-temperature magnetocaloric effect. Additionally, the $Fe_{83}Mo_6Si_1B_7P_2C_1$ amorphous alloy does not contain any rare earth elements and, thus, has the advantage of low cost. The above advantages make the $Fe_{83}Mo_6Si_1B_7P_2C_1$ amorphous alloy a promising candidate as room-temperature magnetic refrigerants.

IV. CONCLUSION

In this work, by optimizing the alloy composition, a new high Fe-content $Fe_{83}Mo_6Si_1B_7P_2C_1$ amorphous alloy with room-temperature magnetocaloric effect was successfully prepared by melt-spinning technique. The $Fe_{83}Mo_6Si_1B_7P_2C_1$ amorphous alloy ribbon exhibits a T_C of 300 K, a J_s of 148 emu/g, a $\lvert\Delta S_M^{max}\rvert$ of 2.74 J kg^{-1} K^{-1}, and a RC of 485.2 J kg^{-1} under an applied field of 5 T. Compared with the reported Fe-based amorphous alloys with near room-temperature magnetocaloric effect so far, the present $Fe_{83}Mo_6Si_1B_7P_2C_1$ amorphous alloy with high Fe content and no any rare earth elements exhibits excellent room-temperature magnetocaloric properties and low material cost and, thus, is expected to be a potential room-temperature magnetic refrigerant.

ACKNOWLEDGMENTS

This research was supported by the National Natural Science Foundation of China (NNSFC) (Grant No. 51771161) and the Tianshan Innovation Team Program of Xinjiang Uygur Autonomous Region (No. 2020D14038).

AUTHOR DECLARATIONS

Conflict of Interest

The authors have no conflicts to disclose.

Author Contributions

Mengqi Gao: Data curation (equal); Formal analysis (equal); Investigation (equal); Writing – original draft (equal). **Lei Xie:** Conceptualization (equal); Validation (equal). **Qiang Li:** Supervision (equal); Writing – review and editing (equal). **Juntao Huo:** Conceptualization (equal); Writing – review and editing (equal). **Chuntao Chang:** Conceptualization (equal); Writing – review and editing (equal).

DATA AVAILABILITY

The data that support the findings of this study are available from the corresponding author upon reasonable request.

REFERENCES

[1]A. Smith, Eur. Phys. J. H **38**(4), 507–517 (2013).
[2]V. K. Pecharsky and K. A. Gschneidner, J. Alloys Compd. **260**, 98–106 (1997).
[3]B. F. Yu, Q. Gao, B. Zhang, X. Z. Meng, and Z. Chen, Int. J. Refrig. **26**(6), 622–636 (2003).
[4]O. Gutfleisch, M. A. Willard, E. Bruck, C. H. Chen, S. G. Sankar, and J. P. Liu, Adv. Mater. **23**(7), 821–842 (2011).
[5]J. Q. Feng, Y. H. Liu, J. H. Sui, A. N. He, W. X. Xia, W. H. Wang, J. Q. Wang, and J. T. Huo, Mater. Today Phys. **21**, 100528 (2021).
[6]V. K. Pecharsky and K. A. Gschneidner, Jr, Phys. Rev. Lett. **78**, 4494 (1997).
[7]M. Katter, V. Zellmann, G. W. Reppel, and K. Uestuener, IEEE Trans. Magn. **44**, 3044 (2008).
[8]L. Caron, N. T. Trung, and E. Bruck, Phys. Rev. B **84**, 020414 (2011).
[9]P. GeRbara and M. Hasiak, J. Appl. Phys. **124**, 083904 (2018).
[10]Q. Luo, D. Q. Zhao, M. X. Pan, and W. H. Wang, Appl. Phys. Lett. **89**(8), 081914 (2006).
[11]W. Yang, J. Huo, H. Liu, J. Li, L. Song, Q. Li, L. Xue, B. Shen, and A. Inoue, J. Alloys Compd. **684**, 29–33 (2016).
[12]A. Łukiewska, J. Olszewski, M. Hasiak, and P. Gębara, Acta Phys. Pol., A **133**, 676–679 (2018).
[13]V. Provenzano, A. J. Shapiro, and R. D. Shull, Nature **429**, 853 (2004).
[14]A. Ukiewska and P. Gbara, Materials **15**(1), 34 (2022).
[15]K. A. Gschneidner and V. K. Pecharsky, Annu. Rev. Mater. Res. **30**, 387–429 (2000).
[16]K. Wu, C. Liu, Q. Li, J. Huo, M. Li, C. Chang, and Y. Sun, J. Magn. Magn. Mater. **489**, 165404 (2019).
[17]K. Narita, H. Fukunaga, and J. Yamasaki, Jpn. J. Appl. Phys. **16**, 2063–2064 (1977).
[18]J. Durand, IEEE Trans. Magn. **12**, 945–947 (1976).
[19]H. L. Yeh and R. Maddin, Metall. Trans. A **10**(7), 771–781 (1979).
[20]A. Kupczyk, J. Swierczek, M. Hasiak, K. Prusik, J. Zbroszczyk, and P. Gebara, J. Alloys Compd. **735**, 253–260 (2018).
[21]T. Hashimoto, T. Numasawa, M. Shino, and T. Okada, Cryogenics **21**(11), 647–653 (1981).
[22]X. Yang, X. Ma, Q. Li, and S. Guo, J. Alloys Compd. **554**, 446–449 (2013).
[23]W. Wang, Prog. Mater. Sci. **52**, 540–596 (2007).
[24]X. C. Zhong, H. C. Tian, S. S. Wang, Z. W. Liu, Z. G. Zheng, and D. C. Zeng, J. Alloys Compd. **633**, 188–193 (2015).
[25]H. Zhang, R. Li, T. Xu, F. Liu, and T. Zhang, J. Magn. Magn. Mater. **347**, 131–135 (2013).
[26]Q. Wang, L. L. Pan, B. Z. Tang, D. Ding, and L. Xia, J. Non-Cryst. Solids **580**, 121394 (2022).
[27]D. Q. Guoa, K. C. Chana, L. Xiab, and P. Yuc, J. Magn. Magn. Mater. **423**, 379–385 (2017).